Unraveling Eumelanin Radical Formation by Nanodiamond Optical Relaxometry in a Living Cell

Qi Lu [a†], Berlind Vosberg [a†], Zhenyu Wang [b,c,d], Priyadharshini Balasubramanian [e], Maabur Sow [e], Carla Volkert [a], Raul Gonzalez Brouwer [e], Ingo Lieberwirth [a], Robert Graf [a], Fedor Jelezko [e*], Martin B. Plenio [b*], Yingke Wu [a*], Tanja Weil [a*]

[†] Q. L and B. V contributed equally

a Max Planck Institute for Polymer Research, Ackermannweg 10, 55128 Mainz, Germany

*E-mail: weil@mpip-mainz.mpg.de, wuyingke@ mpip-mainz.mpg.de

b Institute of Theoretical Physics and Center for Integrated Quantum Science and Technology (IQST), Ulm University, Albert-Einstein-Allee 11, 89081 Ulm, Germany

*E-mail: martin.plenio@uni-ulm.de

c Key Laboratory of Atomic and Subatomic Structure and Quantum Control (Ministry of Education), and School of Physics, South China Normal University, Guangzhou 510006, China

d Guangdong Provincial Key Laboratory of Quantum Engineering and Quantum Materials, and Guangdong-Hong Kong Joint Laboratory of Quantum Matter, South China Normal University, Guangzhou 510006, China

e Institute for Quantum Optics and Center for Integrated Quantum Science and Technology (IQST), Ulm University, Albert-Einstein-Allee 11, 89081 Ulm, Germany

*E-mail: fedor.jelezko@uni-ulm.de

Key words: nanodiamond, eumelanin, free radicals detection, cells, nitrogen-vacancy center, quantum sensor

Abstract

Defect centers in nanodiamond allow the detection of tiny magnetic fields in their direct surrounding, which makes them an emerging tool for nanoscale sensing applications. The abundant pigment eumelanin plays a major role in biology and material science. We present the first time tracking of the comproportionation reaction in eumelanin by detecting and quantifying semiquinone radicals via the nitrogen-vacancy colour centre as single atom detector. A thin layer of eumelanin is polymerized on the surface of NDs and depending on the environmental conditions, such as pH, near infrared and ultraviolet light irradiation, the radicals undergo maintenance, formation, or disappearance in-situ. By combining experiments and theoretical simulations, we were able to quantify the local number and kinetics of free radicals in the eumelanin layer. Next, the nanodiamond sensor was transported into cells in endosomal vesicles and the number of radicals within the eumelanin layer was also determined. The new quantum sensor could provide valuable insights into the chemistry of eumelanin, which could shine light on eumelanin and melanin-related diseases.

Introduction

Melanin is the primary photoprotecting pigment in human and plays a crucial role in shielding our eyes and skin from the harmful effects of sunlight. However, its intricate involvement in various processes extends beyond photoprotection, encompassing pigmentation regulation, efficient free radical scavenging, and even defense against intense radiation.[1-3] There is a great interest to elucidate the chemistry and biology of these pigments within living systems. The structure of the abundant black-brown polymeric pigment eumelanin is very heterogeneous and complex. It contains multiple indolic building blocks, i.e. 5,6-dihydroxyindole and 5,6-dihydroxyindole-2-carboxylic acid, that are covalently as well as non-covalently linked providing a variety of redox-active hydroquinone, quinone methide, quinone imine, and quinone groups.[4] The generation of persistent, stable free radicals appears to be a key feature of eumelanin

physiochemistry.[5, 6] Many studies have been carried out using electron paramagnetic resonance (EPR) spectroscopy to investigate the spin properties of eumelanin in diverse conditions[7-11], and infrared spectroscopy to study the comproportionation reaction of eumelanin[12]. The investigation of the formation of eumelanin radicals in the complex, dynamic and inhomogeneous environment of living cells has not been successful yet, due to the lack of sensitivity of conventional detection methods. Moreover, the amount of free radicals of eumelanin granules in different intracellular locations and at different time points can vary substantially.[13, 14] To gain a more comprehensive understanding of their biological functions in a spatiotemporal context, there is an urgent need for nanoscale characterization tools that allow in-situ real-time detection of the radicals present in eumelanin granules, with a particular emphasis on accurately quantifying the precise number of radicals inside cells.

Fluorescent nanodiamonds (NDs) with nitrogen vacancy (NV^-) centres can sense paramagnetic species such as ferritin,[15] Gd^{3+},[16] radicals,[17-19] due to their unique spin-dependent emission features. Furthermore, compared to conventional fluorescence-based methods of detecting radicals within living cells[20-22], NDs are inert and they do not undergo chemical reactions with locally formed radicals. Since they neither interfere nor react with radicals formed during the detection process,[23] they can outperform fluorescent dyes as probes that react with locally formed radicals[20-22] to correlate radical formation with cellular responses.

The NV^--based quantum sensing methodology is depicted in Scheme 1. The T_1 relaxation time of the NV^- centres in the ND sensor is determined by first initializing the NV^- in the $m_s = 0$ state by using a green laser pulse. Following a variable waiting time τ, the NV^- spin state is read out using a subsequent laser pulse. The T_1 relaxation time is measured using this all-optical relaxometry technique. When NDs were exposed to a fluctuating magnetic field produced by the surrounding radicals, the T_1 relaxation time of NV^- centres is shortened. So a quantitative determination of the concentration of radicals surrounding the ND surface can be achieved with high sensitivity and high spatial resolution.[24]

Herein, we present a ND quantum sensor, termed RGS-ND (radical generation and sensing nanodiamond"), that allows, for the first time, the sensitive in-situ detection of radical species formed in eumelanin in a spatiotemporal manner after

irradiation or at different pH and inside a living cell. Following a previously published protocol,[25] L-DOPA was polymerized at the surface of NDs into a thin and highly cross-linked network, a functional mimic of natural eumelanin.[26, 27] The absolute number of radicals detected by the RGS-ND quantum sensor was quantified at different pH and the kinetics of radical formation was monitored in-situ by theoretical and numerical modelling of the magnetic noise induced by the radicals in the eumelanin network. Subsequently, the method was applied and tested in living cells, and in this way, the in-situ detection of eumelanin radicals in endosomal compartments was also realised. We envision that our method could contribute to the fundamental understanding of eumelanin chemistry and melanin-related cellular activities and diseases such as melanogenesis, and melanoma.[28, 29]

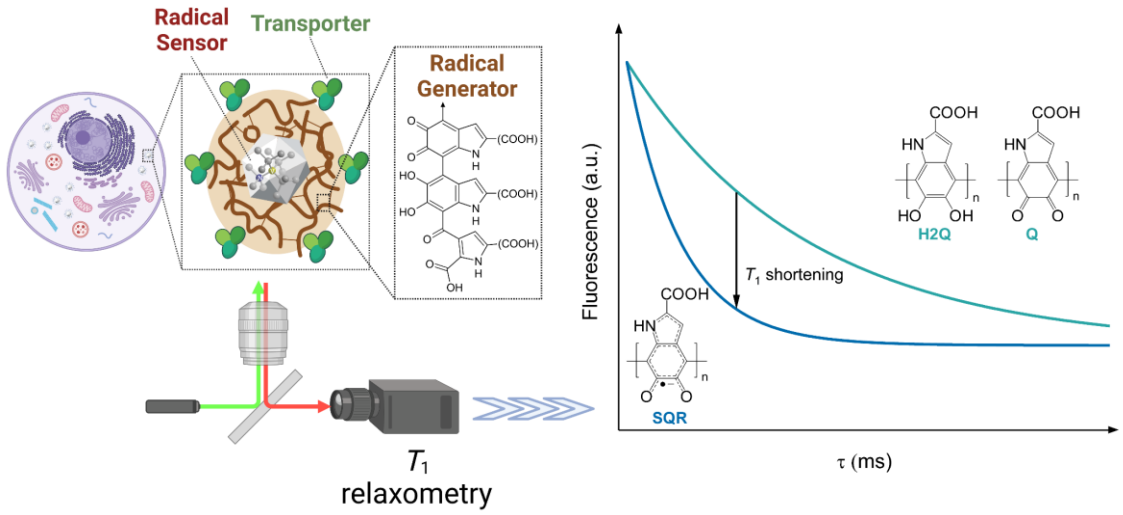

Scheme 1: Detecting free radicals of eumelanin in different media including the living cell. The ND sensor with an eumelanin layer allows radical generation and sensing by fluorescence readout. A transport protein was applied to also facilitate studies inside living cells. The transformation of eumelanin containing quinone (Q) and hydroquinone moieties (H_2Q) to semiquinone radicals (SQR) results in a shortening in T_1 relaxometry, which allows in-situ quantification of radicals in various media including complex living environments.

Results and Discussion

Preparation and characterization of the nanodiamond radical sensor

Fluorescent nanodiamonds (NDs) with sizes from 40 nm to 50 nm were purchased from Adámas Nanotechnologies and used without further surface treatment. In brief, NDs were mixed with L-DOPA in aqueous solution before the $NaIO_4$ solution was added to initiate the oxidation L-DOPA (Figure 1a). After stirring for 15 min, the unreacted agents were removed by centrifugation at 12,000 rpm and washed three times with water to isolate the purified RGS-NDs coated with an eumelanin layer in 23 % yield. The hydrodynamic diameter of the RGS-NDs was assessed by dynamic light scattering (DLS; Figure 1b) and an increase from 33.8 ± 1.7 nm for the uncoated NDs to 43.9 ± 1.1 nm for the RGS-NDs was observed in aqueous media. This corresponds to a thickness of the hydrated eumelanin-solvent layer of about 15 nm.

The coated RGS-NDs were further characterized by transmission electron microscopy (TEM) to image their structure and morphology in the dry state. As shown in Figure 1c, TEM images revealed a uniform thin coating of about 2.0 ± 0.3 nm (n=15) thickness surrounding the RGS-NDs indicating the presence of the eumelanin polymer. To further confirm the eumelanin layer on the surface of the NDs, the attenuated total reflection Fourier transform infrared (ATR-FTIR) spectrum and the absorbance spectrum of RGS-NDs were measured (Figure 1d). The weak intensity peak at 2938 cm^{-1} was attributed to the stretching vibration of aliphatic C-H group.[30, 31] The peak at 1537 cm^{-1} was assigned to the bending vibration of aromatic ring C=C and C=N bonds of the aromatic system in addition to C=O double bonds of carboxylic groups.[32] The aliphatic C-H groups was found at 1451 cm^{-1}. The weak peak at 1382 cm^{-1} could be assigned to the OH bending of phenolic groups, indicating the indole ring vibration.[30] In addition, the absorbance spectrum (Figure S1) of RGS-NDs showed a slight red shift of 5 nm compared to pure NDs due to the phenyl groups in eumelanin layer.

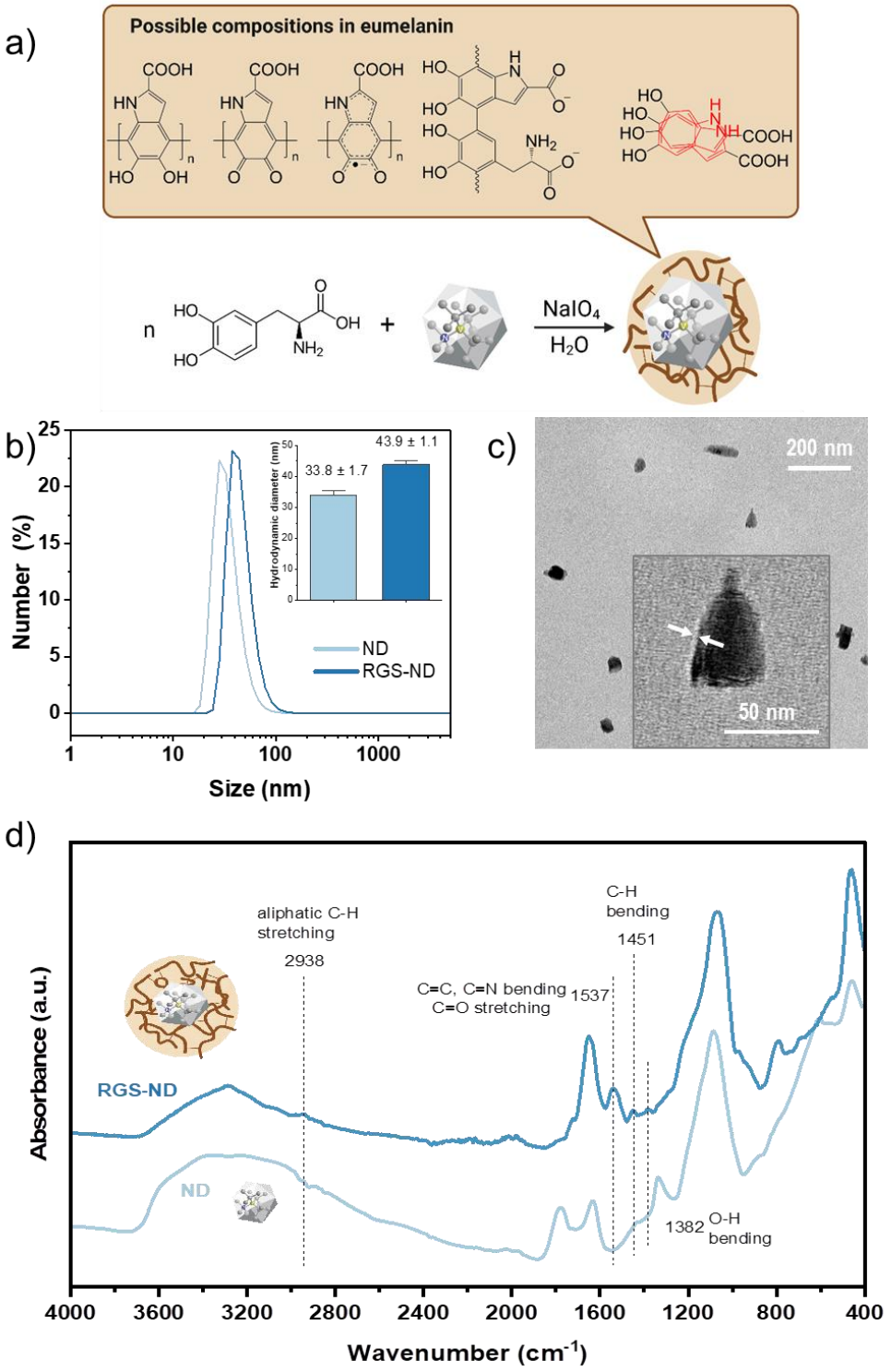

Figure 1. Characterizations of eumelanin modified RGS-NDs. a. Synthesis of NDs. b. Hydrodynamic diameters determined by DLS (Data presented as Mean ± SD). c. TEM image of RGS-NDs, the eumelanin layer was indicated by dashed line. d. ATR-FTIR. 2938 cm^{-1}: aliphatic C-H stretching; 1537 cm^{-1}: aromatic ring C=C and C=N bending in addition to C=O stretching of carboxylic groups; 1451 cm^{-1}: aliphatic C-H bending; 1382 cm^{-1}: phenolic OH bending.

Nanoscale detection of radicals formed in eumelanin by nanodiamond optical relaxometry

At the comproportionation equilibrium of eumelanin, the quinone (Q) and the hydroquinone moieties (H_2Q) can react with water molecules to form hydronium and semiquinone radicals (SQR) as depicted in Figure 2c. In brief, the H_2Q is first deprotonated to form Q^{2-}, followed by an one-electron oxidation that produces the anion SQR[33] that can be detected at the surface of single NDs. To quantify the SQR radicals in the eumelanin layer of RGS-NDs, the longitudinal T_1 relaxation time of the NV^- centre was measured on a home-built optically detected magnetic resonance (ODMR) spectroscope. In brief, the radicals in the eumelanin layer generate a fluctuating magnetic field as noise in the vicinity of the RGS-NDs that shortens the T_1 relaxation time of the NV^- centre, which is measured by optical readout.[34] To perform these measurements, a silicone gasket was placed on top of an O_2-plasma cleaned glass coverslip and the uncoated ND or the coated RGS-ND in aqueous solution were drop-casted into the well, and covered with a removable transparent plastic film to prevent evaporation of the buffer solutions. First, the T_1 relaxation time was determined on single, isolated RGS-NDs based on the confocal images depicted in Figure S2 at different pH. The pulse scheme for measuring the T_1 relaxation time of the NVs is shown in Figure 2a. Subsequently, the T_1 relaxation time was determined by first initializing the NV^- into the $m_s = 0$ state with a green laser pulse. After a variable waiting time τ, the NV^- spin state was read out using a laser pulse to probe spin relaxation from the $m_s = 0$ spin state to the thermally mixed state. In Figure 2b, we plotted the typical T_1 measurements of dry ND (green), RGS-ND in dry condition (blue), and RGS-ND in phosphate buffer at pH 7 (red). For each reaction condition (dry and buffer), the spectral properties of around 20 NDs were measured. We observed that the T_1 relaxation time decreased from 223.9 µs for ND to 66.1 µs for RGS-ND (dry condition) and to 36.1 µs for RGS-ND (phosphate buffer, pH 7.4). These observations are consistent with published work by Meredith et al.[8], in which they investigated changes in radical concentration in an eumelanin film by EPR, indicating that water molecules support radical formation in the eumelanin layer.

Next, the impact of pH on radical formation and the mean T_1 relaxation time in the eumelanin layer of RGS-ND was evaluated. As shown in Figure 2c, the mean T_1 relaxation times of RGS-NDs remained constant (54.4 ± 11.3, 56.2 ± 11.2 µs, n ≥ 16)

at pH 3 and pH 4. This observation is in agreement with EPR data from the literature[35], indicating that the semiquinone radicals form the respective quinone (Q) and catechol (H2Q) groups below pH 5. However, between pH 5 to pH 7, the mean T_1 relaxation time of RGS-ND gradually decreased from 46.6 ± 8.5 (pH 5), 28.9 ± 8.1 (pH 6), to 23.3 ± 5.0 µs (pH 7) reflecting the shift in the comproportionation equilibrium towards the formation of SQRs, which reached saturation at pH 8. Further increase of the pH up to 9.8 did not change the number of semiquinone radicals and the mean T_1 relaxation time remained constant. Above pH 10, eumelanin is known to degrade[36] and therefore, no measurements were performed at higher pH.

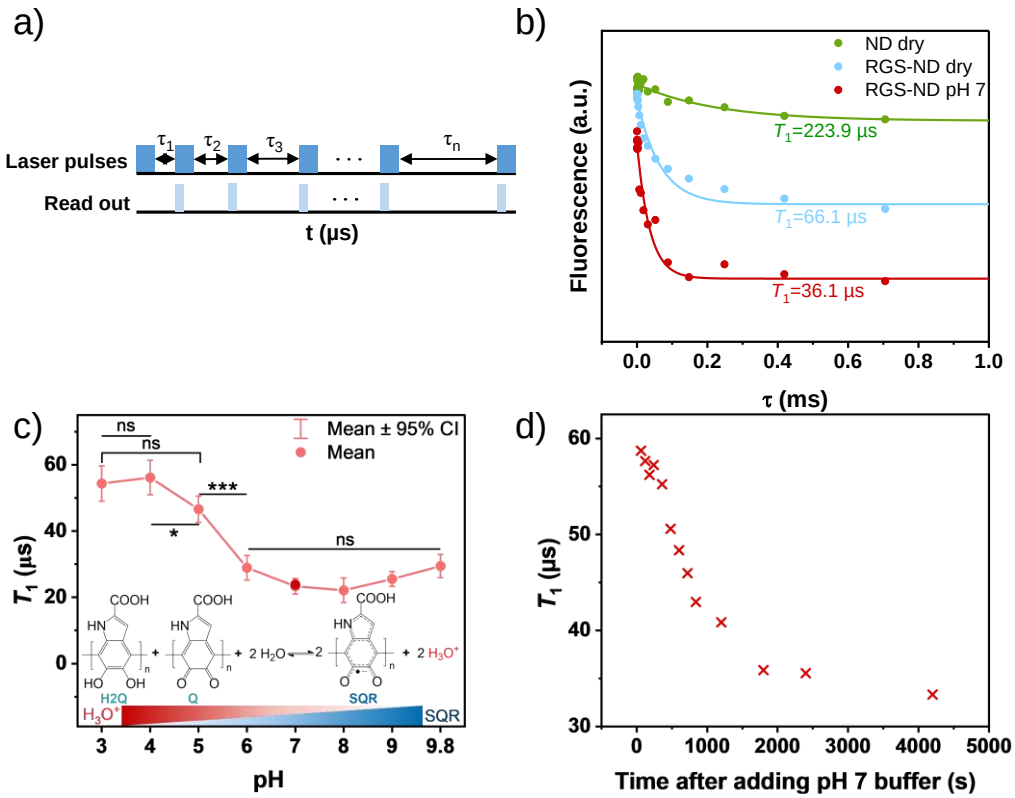

Figure 2. a. Pulse scheme for T_1 measurements. b. Typical T_1 measurement on ND (green), RGS-ND in dry condition (blue), and RGS-ND in phosphate buffer at pH 7 (red), corresponding to Figure 2c at pH 7 and figure 2d. c. T_1 of RGS-ND in phosphate buffer solutions (n≥16). The comproportionation equilibrium of quinone (Q) and hydroquinone (H_2Q) groups to form semiquinone radicals (SQR) is illustrated. d. Kinetics of radical formation quantified by RGS-NDs over time after addition of phosphate buffer (pH 7).

In order to investigate the kinetics of radical formation at pH 7, we conducted T_1 relaxation time measurements of RGS-ND immediately after adding the pH 7 buffer solution and monitored the changes in T_1 over the course of approximately one hour. Within the first 20 minutes after adding the buffer solution, we observed a significant decrease in T_1, which then stabilized at around 35 µs (Figure 2d). This decrease was attributed to the formation of radicals within the eumelanin layer, which occurred immediately after the reaction was initiated by adding the buffer solution and remained constant after 20 min. These results may indicate that it takes about 20 minutes for a stable comproportionation equilibrium to form within the eumelanin shell. Perhaps, the highly crosslinked eumelanin layer has an impact on the diffusion of water molecules required for the formation of hydronium and semiquinone radicals (SQR) at neutral pH. As comparison, we also recorded the EPR spectrum of RGS-NDs (Figure S3), but the signal-to-noise ratio was too low i.e. compared to the stable (2,2,6,6-tetramethylpiperidin-1-yl)oxidanyl (TEMPO) radical, thus highlighting the considerably higher sensitivity of T_1 relaxometry compared to bulk EPR.[37]

Nanoscale detection of local temperature changes by nanodiamond optical relaxometry

Melanin can reduce the risk of skin cancer through transforming the absorbed sunlight energy into heat.[38, 39] Therefore, the influence of local temperature fluctuations on the RGS-NDs was investigated first by measuring on the T_1 relaxation time under NIR irradiation (810 nm, 350 mW/cm^2) for 10 minutes, because the T_1 relaxation time only shows temperature-dependency at cryogenic temperatures. Noteworthy, only the formation of SQ radicals within the eumelanin shell will shorten the T_1 relaxation time in our setup.[40] RGS-NDs in water and in the dry state were irradiated for 10 min and the T_1 relaxation times remained constant for more than 20 min minutes as depicted in Figure S4. Next, the mean T_1 relaxation times of RGS-NDs were measured under higher energy UV irradiation (365 nm, 0.3 mW/cm^2) of 10 min, and the corresponding results were presented in Figure S5. No significant changes were observed with or without irradiation with UV and NIR light, indicating that RGS-ND selectively responds to changes in local radical formation, while UV radiation and potential local temperature gradients[41] did not interfere with radical sensing in our experimental setup.

Quantification of radical formation in the eumelanin shell of RGS-NDs by theoretical simulation of spin relaxation times

From the T_1 relaxation times, we can estimate the exact number of radicals in the shell of RGS-NDs. To this end, we employed a theoretical model[17, 24, 42] to simulate the T_1 relaxation times for different radical concentrations in the eumelanin shell. The radicals in the polymer layer produce a fluctuating magnetic field at the position of the NV$^-$ centre, which is characterized by an amplitude variance $B_\perp^2$ and a temporal correlation time τ_c. Increasing concentrations and numbers of radicals produce a stronger noise amplitude which induced shortening of the T_1 relaxation time. Let T_1^{other} be the NV$^-$ spin relaxation time without the radicals in the shell of RGS-ND, the overall T_1 is determined by

$$\frac{1}{T_1} = \frac{1}{T_1^{\text{other}}} + \frac{1}{T_1^{\text{radical}}},$$

where $\frac{1}{T_1^{\text{radical}}} = 3\gamma_e^2 B_\perp^2 \frac{\tau_c}{1+(\omega_{\text{NV}}\tau_c)^2}$ is the radical induced relaxation rate of an NV$^-$ centre with a resonance frequency $\omega_{\text{NV}} \approx 2\pi \times 2.87$ GHz. To simulate $B_\perp^2$ and τ_c, we assumed that each ND has a spherical shape and the 14 inner NV$^-$ centres have random locations and orientations. We assume that the NV$^-$ centres are located at least 2 nm below the diamond surface as shallower NV$^-$ centres are not stable. The shell of RGS-ND has a thickness of 2 nm. Due to vibrational relaxation and inter-radical flip-flop interactions, the magnetic field from each radical in the shell will fluctuate and contribute to the total magnetic field amplitude variance $B_\perp^2 = \Sigma_j {B_\perp}_{,j}^2$. Here the radical and the NV$^-$ have a relative distance of $r_{c,j}$ and an orientation $\hat{r}_{c,j}$. μ_0 is the vacuum permeability, γ_e is the electron gyromagnetic ratio, and the unit vector $\hat{z}$ denotes the NV$^-$ symmetry axis. In our model, we consider surface electrons at the ND surface, which generate magnetic noise in a similar manner as the radicals in the shell of RGS-ND and contribute spin relaxation in $\frac{1}{T_1^{\text{other}}}$ (see Supporting Information for details of the model).

$$B_{\perp,j}^2 = \frac{1}{4}\left(\frac{\mu_0\gamma_e}{4\pi}\right)^2 \left(\frac{5 - 3\left(\hat{r}_{c,j}\cdot\hat{z}\right)^2}{r_{c,j}^6}\right),$$

We performed Monte Carlo simulation for 1000 ND samples, where the NV$^-$ centre has random location and orientation. We firstly determined the density of surface

electrons to match the experimentally observed average T_1^{other} of 223.9 μs. Then, we added radicals to the 2 nm shell of RGS-ND so that the average T_1 reaches the values in Figure. 2c. From the corresponding radical densities, we can estimate the number of radicals at different pH values as shown in Figure. 3. The number of radicals in the layer of eumelanin were increasing from pH 4 to pH 8 and we could estimate about 4992 (pH 3), 4777 (pH 4), 6113 (pH 5), 10929 (pH 6), 13992 (pH 7), 14853 (pH 8), 12627 (pH 9), and 10713 (pH 9.8) radicals per RGS-ND.

Moreover, assuming that one L-DOPA monomer could in principle form one SQR, one could roughly estimate that at least 14853 L-DOPA monomers are present in the eumelanin shell. As not every L-DOPA monomer likely forms an SQR, the actual number of L-DOPA monomers that formed the eumelanin layer around the RGS-NDs will likely be higher.

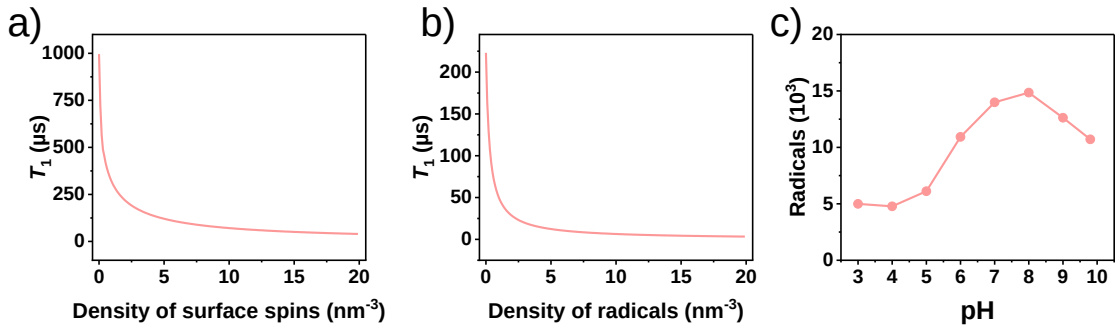

Figure 3. a. Original T_1 time as a function of the density of noise spins on the diamond surface, which was assumed to have a 0.1 nm thick shell (intrinsic thickness of spin on nanodimonds). To have an average T_1 of 223.9 µs for NDs with a diameter of about 27.9 nm, this density of electron spins is $\rho_{\text{noise}} = 1.9/\text{nm}^3$ b. With $\rho_{\text{noise}} = 1.9/\text{nm}^3$ of the density of the noisy electron spins on the surface in (a), the T_1 time as a function of the density of the electron spins in the outer 2-nm-thick coating. c. Estimated number of radicals in eumelanin layer for different pH values. The radical numbers reproduce simulated average T_1 times that match the ones in Figure. 2c, for samples of NDs which have a diameter of 27.9 nm and contain an NV^- centre of random position and orientations. See Supporting Information for details of the model and simulation.

Quantification of radical formation in the eumelanin shell of RGS-NDs in living cells

Nanodiamond quantum sensing provides the unique opportunity to accurately assess the physical and chemical parameters in warm, wet and noisy environments and even in complex systems such as living cells.[43] However, without coating with a cationic surface shell or cell surface receptor ligands, NDs are not uptaken into cells. Therefore, RGS-NDs were incubated with cationic human serum albumin (cHSA), an established transporter protein that facilitates cellular uptake by clathrin-mediated endocytosis and adsorbs to NDs by forming stable complexes.[44-46] The cHSA-RGS-NDs were prepared simply by mixing 400 µg cHSA and 100 µL 1 mg/mL RGD-ND for 30 minutes at room temperature (Figure 4a, see SI for details). After purification by three cycles of centrifugation/suspension (yield: 5.7%), the cHSA-RGS-ND was characterized by ATR-FTIR, DLS and zeta potential (see Figure S6). The hydrodynamic diameter in water increased from 43.9 ± 1.1 nm to 68.0 ± 8.0 nm, while the zeta potential changed from - 33.3 ± 1.7 mV for RGS-NDs to + 18.3 ± 0.1 mV for the cHSA-RGS-NDs, indicating the formation of nanoparticles with positive net charges due to the adsorption of positively charged cHSA. Moreover, the cHSA-RGS-ND is further characterized by ATR-FTIR, the characteristic peaks of amide I and II bonds of cHSA at 1645 and 1543 cm^{-1}, respectively, were clearly observed (Figure S6) indicating successful cHSA coating.

We then tested the radical generating and sensing ability of the cHSA-RGS-ND at pH 4 to 7 buffer solutions over a pH range reflecting the physiological pH in living cells. Before starting the measurement in buffers, we waited for more than 20 min to reach the equilibrium. Similar to RGS-NDs, cHSA-RGS-NDs revealed a decrease in T_1 with increasing pH (Figure 4b, c & S7). The mean T_1 relaxation times dropped from 76.0 ± 26.4 µs (pH 4), 52.8 ± 24.6 µs (pH 5), 31.0 ± 19.5 µs (pH 6) to 27.5 ± 11.5 µs (pH 7) in phosphate buffer solutions. Based on the simulation in Figure 3, we then quantified the number of local radicals that were generated at different pH and 3193 (pH 4), 5213 (pH 5), 9711 (pH 6), and 11462 (pH 7) radicals were detected by the NDs, respectively. These experimental data correspond well to the data depicted in Figure 2c, also suggesting that cHSA coating did not affect nor compromise the radical generation and sensing capabilities of cHSA-RGS-NDs.

To study radical formation within the eumelanin layer in living cells, cHSA-RGS-NDs were introduced to the J774A.1 macrophage cell line to achieve better internalization of cHSA-RGS-NDs. After 4 hours of incubation, the cells were washed three times with Dulbecco's Balanced Salt Solution and they were maintained in colorless Leibovitz's L-15 medium for immediate measurement of the T_1 relaxation time of cHSA-RGS-NDs, which was measured on a home-built confocal microscope as described in SI. In brief, the T_1 time was determined by first initializing the NV to the ms = 0 state by using a green laser pulse. Following a variable waiting time τ, the NV spin state was readout using a subsequent laser pulse. A mean T_1 of 72.2 ± 31.0 µs was recorded (Figure 4e) corresponding to about 3301 radicals formed within the eumelanin layer of intracellular RGS-NDs. TEM images of the cHSA-RGS-NDs revealed that the nanoparticles remained in vesicles (Figure S8), which corresponds to previous data.[47] Based on the observed number of radicals in the eumelanin layer, the intracellular pH value in the surrounding of the cHSA-RGS-NDs could be estimated. The pH between 4 and 5 indicated that the cHSA-RGS-NDs were localized in lysosomal compartments with typical pH between 4.5–5[48-50] compared to early (pH 6.5) or late (pH 5.5) endosomal vesicles or the cytosolic pH of 7–7.5. Thus, the T_1 relaxation time insinuated a lysosomal localization of cHSA-RGS-NDs.

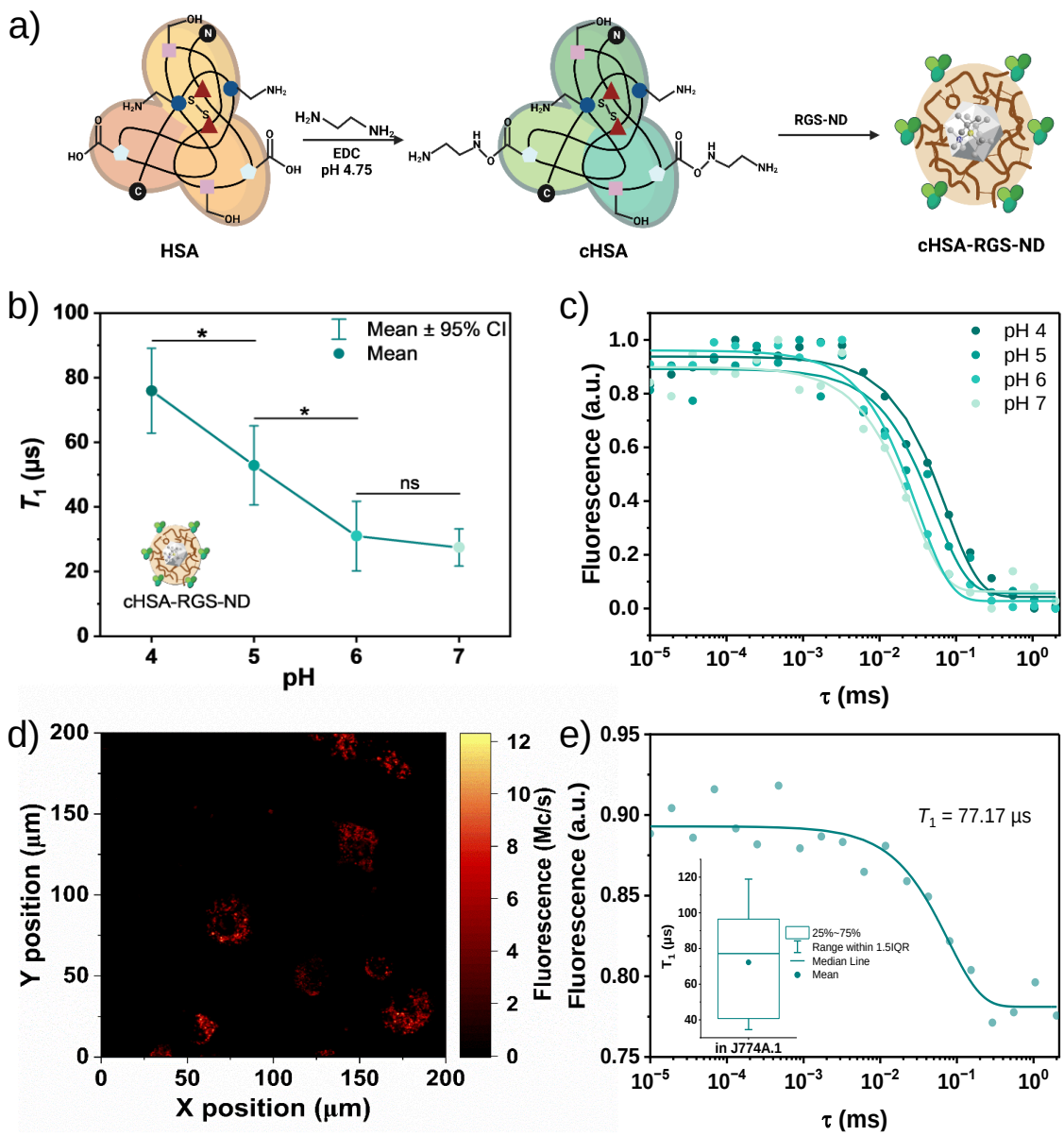

Figure 4. a. Synthesis of cHSA-RGS-ND. b. T_1 relaxation time of cHSA-RGS-ND in pH 4-7 buffer solutions (n≥15). c. Typical T_1 measurement of cHSA-RGS-ND in pH 4-7 buffer solutions. d. X – Y axis confocal microscopy images of cHSA-RGS-ND taken up into J774A.1 cells at 100 μg/mL after 4 hours incubation. e. Representative T_1 decay of cHSA-RGS-ND in macrophages, inserted is a box chart of T_1 of internalized cHSA-RGS-NDs.

Conclusion

In conclusion, we have polymerized eumelanin on the surface of a nanodiamond quantum sensor. Due to the intrinsic sensitivity of the NV^- quantum sensor to magnetic

field fluctuations, these NDs could serve as nanoscale sensor that is capable of quantitatively measuring the amount of radical species in eumelanin. This is even possible at the level of individual cells, a regime inaccessible to standard EPR spectroscopy at such low radical levels. Combining the measured T_1 reduction with theoretical simulations, we demonstrate that the number of radicals formed in the eumelanin layer is pH dependent. We could quantify the number of radicals at different pH (3, 4, 5, 6, 7, 8, 9, 9.8), which increased from 4777 surface radicals at pH 4 to 14853 radicals at pH 8, respectively. Although the number of radicals in eumelanin increased for higher pH, these measurements were not affected by other parameters such as temperature changes due to UV or NIR irradiation.

Therefore, by using the highly sensitive T_1 relaxometry, we successfully monitored the chemical reaction in a few nanometer-thick eumelanin layer for the first time. Compared to the widely used EPR spectroscopy, which can provide valuable information about the presence and nature of paramagnetic species in various systems at a macroscopic level, we believe that T_1 relaxometry could become a valuable tool to study chemical reactions that involve paramagnetic species at a nanoscale confined space that is not accessible for conventional techniques such as EPR spectroscopy.

In vitro cell studies were performed and we could quantify the number of radicals within the eumelanin shell even in a single living cell. To date, it has not been possible to detect the radical species in eumelanin with single cell resolution. Therefore, we expect our method to shed light on the role of eumelanin in pigmentation, free radical scavenging, and anti-oxidation. It could provide insights into melanin-related disease and facilitate the development of effective medical interventions.

Author contributions

Qi Lu, Yingke Wu: Methodology, Investigation, Writing—original draft and editing. Berlind Vosberg: Methodology, Investigation, Yingke Wu: Conceptualization and Supervision. Zhenyu Wang: Simulation. Priyadharshini Balasubramanian, Maabur Sow, Raúl Gonzalez Brouwer: ODMR set-up, Software for data acquisition. Ingo Lieberwirth: TEM Investigation. Carla Volkert, Robert Graf: EPR Investigation. Fedor

Jelezko, Martin B. Plenio, Tanja Weil: Conceptualization, Supervision, Funding acquisition, Writing—review and editing.

Conflicts of interest

The authors declare no competing financial interest.

Supporting Information

Supporting Information is available from…

Acknowledgements

The authors thank Christoph Sieber for preparing TEM samples of cells, Md Noor A Alam for preparing cHSA, Tommaso Marchesi D'Alvise for many helpful discussions, Mirja Harms and Jan Münch for providing cell culture facilities at Ulm University. T. Weil is grateful for the financial support from the Deutsche Forschungsgemeinschaft (DFG, German Research Foundation) - Project number 316249678 - SFB 1279 (C04). M.B. Plenio acknowledges support from the European Research Council via Synergy grant HyperQ (grant no. 856432) and the Bundesministerium für Bildung und Forschung (BMBF) via the project QSens: Quantensensoren für die biomedizinische Diagnostik (QMED) (grant no. 03ZU1110FF). Z. Wang acknowledges supports from the National Natural Science Foundation of China (Grant No. 12074131) and the Natural Science Foundation of Guangdong Province (Grant No. 2021A1515012030). F. Jelezko acknowledge the support of Federal Ministry of Education and Research BMBF, ERC (Synergy Grant HyperQ), European Commission (Projects FLORIN, QCIRCLE), DFG (Excellence Cluster POLiS, CRC 1279, and projects 499424854, 387073854) and Carl Zeiss Stiftung.

References

(1) Lin, J. Y.; Fisher, D. E. Melanocyte biology and skin pigmentation. *Nature* **2007**, *445* (7130), 843-850. DOI: 10.1038/nature05660.
(2) Sarna, T.; Pilas, B.; Land, E. J.; Truscott, T. G. Interaction of radicals from water radiolysis with melanin. *Biochim. Biophys. Acta.* **1986**, *883* (1), 162-167. DOI: 10.1016/0304-4165(86)90147-9.
(3) Abbas, K.; Qadir, M. I.; Anwar, S. The Role of Melanin in Skin Cancer. *Crit. Rev. Eukaryot. Gene Expr.* **2019**, *29* (1), 17-24. DOI: 10.1615/CritRevEukaryotGeneExpr.2018024980.
(4) Cao, W.; Zhou, X.; McCallum, N. C.; Hu, Z.; Ni, Q. Z.; Kapoor, U.; Heil, C. M.; Cay, K. S.; Zand, T.; Mantanona, A. J.; et al. Unraveling the Structure and Function of Melanin through Synthesis. *J. Am. Chem. Soc.* **2021**, *143* (7), 2622-2637. DOI: 10.1021/jacs.0c12322.
(5) Meredith, P.; Sarna, T. The physical and chemical properties of eumelanin. *Pigment Cell Res.* **2006**, *19* (6), 572-594. DOI: 10.1111/j.1600-0749.2006.00345.x.
(6) Slominski, A.; Tobin, D. J.; Shibahara, S.; Wortsman, J. Melanin Pigmentation in Mammalian Skin and Its Hormonal Regulation. *Physiol. Rev.* **2004**, *84* (4), 1155-1228. DOI: 10.1152/physrev.00044.2003.
(7) Manini, P.; Margari, P.; Pomelli, C.; Franchi, P.; Gentile, G.; Napolitano, A.; Valgimigli, L.; Chiappe, C.; Ball, V.; d'Ischia, M. Nanoscale Disassembly and Free Radical Reorganization of Polydopamine in Ionic Liquids. *J. Phys. Chem. B* **2016**, *120* (46), 11942-11950. DOI: 10.1021/acs.jpcb.6b08835.
(8) Mostert, A. B.; Rienecker, S. B.; Noble, C.; Hanson, G. R.; Meredith, P. The photoreactive free radical in eumelanin. *Sci. adv.* **2018**, *4* (3), eaaq1293. DOI: 10.1126/sciadv.aaq1293.
(9) Paulin, J. V.; Batagin-Neto, A.; Graeff, C. F. O. Identification of Common Resonant Lines in the EPR Spectra of Melanins. *J. Phys. Chem. B* **2019**, *123* (6), 1248-1255. DOI: 10.1021/acs.jpcb.8b09694.
(10) Zou, Y.; Chen, X.; Yang, P.; Liang, G.; Yang, Y.; Gu, Z.; Li, Y. Regulating the absorption spectrum of polydopamine. *Sci. Adv.* **2020**, *6* (36), eabb4696. DOI: 10.1126/sciadv.abb4696.
(11) Mignion, L.; Desmet, C. M.; Harkemanne, E.; Tromme, I.; Joudiou, N.; Wehbi, M.; Baurain, J. F.; Gallez, B. Noninvasive detection of the endogenous free radical melanin in human skin melanomas using electron paramagnetic resonance (EPR). *Free Radic. Biol. Med.* **2022**, *190*, 226-233. DOI: 10.1016/j.freeradbiomed.2022.08.020.
(12) Bedran, Z. V.; Zhukov, S. S.; Abramov, P. A.; Tyurenkov, I. O.; Gorshunov, B. P.; Mostert, A. B.; Motovilov, K. A. Water-Activated Semiquinone Formation and Carboxylic Acid Dissociation in Melanin Revealed by Infrared Spectroscopy. *Polymers (Basel)* **2021**, *13* (24). DOI: 10.3390/polym13244403.
(13) Paulin, J. V.; Graeff, C. F. O. From nature to organic (bio)electronics: a review on melanin-inspired materials. *J. Mater. Chem. C* **2021**, *9* (41), 14514-14531, 10.1039/D1TC03029A. DOI: 10.1039/D1TC03029A.
(14) Dubey, S.; Roulin, A. Evolutionary and biomedical consequences of internal melanins. *Pigment Cell Melanoma Res.* **2014**, *27* (3), 327-338. DOI: 10.1111/pcmr.12231.
(15) Ermakova, A.; Pramanik, G.; Cai, J. M.; Algara-Siller, G.; Kaiser, U.; Weil, T.; Tzeng, Y. K.; Chang, H. C.; McGuinness, L. P.; Plenio, M. B.; et al. Detection of a few metallo-protein molecules using color centers in nanodiamonds. *Nano Lett.* **2013**, *13* (7), 3305-3309. DOI: 10.1021/nl4015233.
(16) Kaufmann, S.; Simpson, D. A.; Hall, L. T.; Perunicic, V.; Senn, P.; Steinert, S.; McGuinness, L. P.; Johnson, B. C.; Ohshima, T.; Caruso, F.; et al. Detection of atomic spin labels in a lipid bilayer using a single-spin nanodiamond probe. *Proc. Natl. Acad. Sci. U.S.A* **2013**, *110* (27), 10894-10898. DOI: 10.1073/pnas.1300640110.
(17) Wu, Y.; Balasubramanian, P.; Wang, Z.; Coelho, J. A. S.; Prslja, M.; Siebert, R.; Plenio, M. B.; Jelezko, F.; Weil, T. Detection of Few Hydrogen Peroxide Molecules Using Self-Reporting Fluorescent Nanodiamond Quantum Sensors. *J. Am. Chem. Soc.* **2022**, *144* (28), 12642–12651. DOI: 10.1021/jacs.2c01065.
(18) Reyes-San-Martin, C.; Hamoh, T.; Zhang, Y.; Berendse, L.; Klijn, C.; Li, R.; Llumbet, A. E.; Sigaeva, A.; Kawałko, J.; Mzyk, A.; et al. Nanoscale MRI for Selective Labeling and Localized Free Radical

Measurements in the Acrosomes of Single Sperm Cells. *ACS Nano* **2022**, *16* (7), 10701-10710. DOI: 10.1021/acsnano.2c02511.
(19) Nie, L.; Nusantara, A. C.; Damle, V. G.; Sharmin, R.; Evans, E. P. P.; Hemelaar, S. R.; van der Laan, K. J.; Li, R.; Perona Martinez, F. P.; Vedelaar, T.; et al. Quantum monitoring of cellular metabolic activities in single mitochondria. *Sci. Adv.* **2021**, *7* (21), eabf0573. DOI: 10.1126/sciadv.abf0573.
(20) Bai, X.; Huang, Y.; Lu, M.; Yang, D. HKOH-1: A Highly Sensitive and Selective Fluorescent Probe for Detecting Endogenous Hydroxyl Radicals in Living Cells. *Angew. Chem. Int. Ed.* **2017**, *56* (42), 12873-12877. DOI: 10.1002/anie.201705873.
(21) Yang, D.; Wang, H. L.; Sun, Z. N.; Chung, N. W.; Shen, J. G. A highly selective fluorescent probe for the detection and imaging of peroxynitrite in living cells. *J. Am. Chem. Soc.* **2006**, *128* (18), 6004-6005. DOI: 10.1021/ja0603756.
(22) Zhang, R.; Zhao, J.; Han, G.; Liu, Z.; Liu, C.; Zhang, C.; Liu, B.; Jiang, C.; Liu, R.; Zhao, T.; et al. Real-Time Discrimination and Versatile Profiling of Spontaneous Reactive Oxygen Species in Living Organisms with a Single Fluorescent Probe. *J. Am. Chem. Soc.* **2016**, *138* (11), 3769-3778. DOI: 10.1021/jacs.5b12848.
(23) Wu, Y.; Jelezko, F.; Plenio, M. B.; Weil, T. Diamond Quantum Devices in Biology. *Angew. Chem. Int. Ed.* **2016**, *55* (23), 6586-6598. DOI: 10.1002/anie.201506556.
(24) Barton, J.; Gulka, M.; Tarabek, J.; Mindarava, Y.; Wang, Z.; Schimer, J.; Raabova, H.; Bednar, J.; Plenio, M. B.; Jelezko, F.; et al. Nanoscale Dynamic Readout of a Chemical Redox Process Using Radicals Coupled with Nitrogen-Vacancy Centers in Nanodiamonds. *ACS Nano* **2020**, *14* (10), 12938-12950. DOI: 10.1021/acsnano.0c04010.
(25) Harvey, S.; Raabe, M.; Ermakova, A.; Wu, Y.; Zapata, T.; Chen, C.; Lu, H.; Jelezko, F.; Ng, D. Y.; Weil, T. Transferrin-Coated Nanodiamond–Drug Conjugates for Milliwatt Photothermal Applications. *Adv. Therap.* **2019**, *2* (11), 1900067. DOI: 10.1002/adtp.201900067.
(26) Gaeta, M.; Barcellona, M.; Purrello, R.; Fragalà, M. E.; D'Urso, A. Hybrid Porphyrin/DOPA-melanin film as self-assembled material and smart device for dye-pollutant removal in water. *Chem. Eng. J.* **2022**, *433*, 133262. DOI: 10.1016/j.cej.2021.133262.
(27) Dai, M.; Huang, T.; Chao, L.; Tan, Y.; Chen, C.; Meng, W.; Xie, Q. Tyrosinase-catalyzed polymerization of l-DOPA (versusl-tyrosine and dopamine) to generate melanin-like biomaterials for immobilization of enzymes and amperometric biosensing. *RSC Adv.* **2016**, *6* (21), 17016-17022. DOI: 10.1039/c5ra27478h.
(28) Slominski, R. M.; Sarna, T.; Płonka, P. M.; Raman, C.; Brożyna, A. A.; Slominski, A. T. Melanoma, Melanin, and Melanogenesis: The Yin and Yang Relationship. *Front. Oncol.* **2022**, *12*, 842496. DOI: 10.3389/fonc.2022.842496.
(29) Riley, P. A. Melanogenesis and melanoma. *Pigment Cell Res.* **2003**, *16* (5), 548-552. DOI: 10.1034/j.1600-0749.2003.00069.x.
(30) Centeno, S. A.; Shamir, J. Surface enhanced Raman scattering (SERS) and FTIR characterization of the sepia melanin pigment used in works of art. *J. Mol. Struct.* **2008**, *873* (1-3), 149-159. DOI: 10.1016/j.molstruc.2007.03.026.
(31) Tarangini, K.; Mishra, S. Production, Characterization and Analysis of Melanin from Isolated Marine Pseudomonas sp. using Vegetable waste. *Res. J. Engineering Sci.* **2013**, *Vol. 2(5)*, 40-46.
(32) Mbonyiryivuze, A.; Mwakikunga, B.; Dhlamini, S. M.; Maaza, M. Fourier Transform Infrared Spectroscopy for Sepia Melanin. *Physics and Materials Chemistry* **2015**, *3* (2), 25-29. DOI: 10.12691/pmc-3-2-2.
(33) Pedersen, J. A. On the application of electron paramagnetic resonance in the study of naturally occurring quinones and quinols. *Spectrochim. Acta A* **2002**, *58* (6), 1257-1270. DOI: 10.1016/S1386-1425(01)00715-6.
(34) Steinert, S.; Ziem, F.; Hall, L.; Zappe, A.; Schweikert, M.; Götz, N.; Aird, A.; Balasubramanian, G.; Hollenberg, L.; Wrachtrup, J. Magnetic spin imaging under ambient conditions with sub-cellular resolution. *Nat. Commun.* **2013**, *4*, 1607. DOI: 10.1038/ncomms2588.

(35) Lin, Q.; Li, Q.; Batchelor-McAuley, C.; Compton, R. G. Two-electron, two-proton oxidation of catechol: kinetics and apparent catalysis. *J. Phys. Chem. C* **2015**, *119* (3), 1489-1495. DOI: 10.1021/jp511414b.
(36) Yang, W.; Liu, C.; Chen, Y. Stability of polydopamine coatings on gold substrates inspected by surface plasmon resonance imaging. *Langmuir* **2018**, *34* (12), 3565-3571. DOI: 10.1021/acs.langmuir.7b03143.
(37) Grinolds, M. S.; Hong, S.; Maletinsky, P.; Luan, L.; Lukin, M. D.; Walsworth, R. L.; Yacoby, A. Nanoscale magnetic imaging of a single electron spin under ambient conditions. *Nature Phys.* **2013**, *9* (4), 215-219. DOI: 10.1038/nphys2543.
(38) Ye, Y.; Wang, C.; Zhang, X.; Hu, Q.; Zhang, Y.; Liu, Q.; Wen, D.; Milligan, J.; Bellotti, A.; Huang, L.; et al. A melanin-mediated cancer immunotherapy patch. *Sci. Immunol.* **2017**, *2* (17), eaan5692. DOI: 10.1126/sciimmunol.aan5692.
(39) Liu, Y.; Ai, K.; Liu, J.; Deng, M.; He, Y.; Lu, L. Dopamine-melanin colloidal nanospheres: an efficient near-infrared photothermal therapeutic agent for in vivo cancer therapy. *Adv. Mater.* **2013**, *25* (9), 1353-1359. DOI: 10.1002/adma.201204683.
(40) de Guillebon, T.; Vindolet, B.; Roch, J. F.; Jacques, V.; Rondin, L. Temperature dependence of the longitudinal spin relaxation time T_1 of single nitrogen-vacancy centers in nanodiamonds. *Phys. Rev. B* **2020**, *102* (16), 165427. DOI: 10.1103/PhysRevB.102.165427.
(41) Sotoma, S.; Zhong, C.; Kah, J. C. Y.; Yamashita, H.; Plakhotnik, T.; Harada, Y.; Suzuki, M. In situ measurements of intracellular thermal conductivity using heater-thermometer hybrid diamond nanosensors. *Sci. Adv.* **2021**, *7* (3), eabd7888. DOI: 10.1126/sciadv.abd7888.
(42) Tetienne, J.-P.; Hingant, T.; Rondin, L.; Cavaillès, A.; Mayer, L.; Dantelle, G.; Gacoin, T.; Wrachtrup, J.; Roch, J.-F.; Jacques, V. Spin relaxometry of single nitrogen-vacancy defects in diamond nanocrystals for magnetic noise sensing. *Phys. Rev. B* **2013**, *87* (23), 235436. DOI: 10.1103/PhysRevB.87.235436.
(43) Wu, Y.; Weil, T. Recent Developments of Nanodiamond Quantum Sensors for Biological Applications. *Adv. Sci.* **2022**, *9*, 2200059. DOI: 10.1002/advs.202200059.
(44) Eisele, K.; Gropeanu, R. A.; Zehendner, C. M.; Rouhanipour, A.; Ramanathan, A.; Mihov, G.; Koynov, K.; Kuhlmann, C. R. W.; Vasudevan, S. G.; Luhmann, H. J.; et al. Fine-tuning DNA/albumin polyelectrolyte interactions to produce the efficient transfection agent cBSA-147. *Biomater.* **2010**, *31* (33), 8789-8801. DOI: 10.1016/j.biomaterials.2010.07.088.
(45) Wu, Y.; Ihme, S.; Feuring-Buske, M.; Kuan, S. L.; Eisele, K.; Lamla, M.; Wang, Y.; Buske, C.; Weil, T. A Core–Shell Albumin Copolymer Nanotransporter for High Capacity Loading and Two-Step Release of Doxorubicin with Enhanced Anti-Leukemia Activity. *Adv. Healthc. Mater.* **2013**, *2* (6), 884-894. DOI: 10.1002/adhm.201200296.
(46) Wu, Y.; Ermakova, A.; Liu, W.; Pramanik, G.; Vu, T. M.; Kurz, A.; McGuinness, L.; Naydenov, B.; Hafner, S.; Reuter, R.; et al. Programmable Biopolymers for Advancing Biomedical Applications of Fluorescent Nanodiamonds. *Adv. Funct. Mater.* **2015**, *25* (42), 6576-6585. DOI: 10.1002/adfm.201502704.
(47) Wu, Y.; Alam, M. N. A.; Balasubramanian, P.; Ermakova, A.; Fischer, S.; Barth, H.; Wagner, M.; Raabe, M.; Jelezko, F.; Weil, T. Nanodiamond Theranostic for Light-Controlled Intracellular Heating and Nanoscale Temperature Sensing. *Nano Lett.* **2021**, *21* (9), 3780-3788. DOI: 10.1021/acs.nanolett.1c00043.
(48) Li, S. S.; Zhang, M.; Wang, J. H.; Yang, F.; Kang, B.; Xu, J. J.; Chen, H. Y. Monitoring the Changes of pH in Lysosomes during Autophagy and Apoptosis by Plasmon Enhanced Raman Imaging. *Anal. Chem.* **2019**, *91* (13), 8398-8405. DOI: 10.1021/acs.analchem.9b01250.
(49) Nowak-Lovato, K. L.; Wilson, B. S.; Rector, K. D. SERS nanosensors that report pH of endocytic compartments during FcepsilonRI transit. *Anal. Bioanal. Chem.* **2010**, *398* (5), 2019-2029. DOI: 10.1007/s00216-010-4176-8.

(50) Ohkuma, S.; Poole, B. Fluorescence probe measurement of the intralysosomal pH in living cells and the perturbation of pH by various agents. *Proc. Natl. Acad. Sci. U.S.A* **1978**, *75* (7), 3327-3331. DOI: 10.1073/pnas.75.7.3327